

Benchmarking Density Functional Approximations, Atomic Basis Sets, and Solvent Models in Predicting Thermodynamic Hydricities in Organic and Organometallic Species

Minh Nguyen and Lee-Ping Wang

Department of Chemistry

University of California, Davis

Submitted May 20, 2019

Abstract

The hydricity (ΔG_{H^-}) is a molecular property that measures the thermodynamic ability to donate a hydride ion, H^- , and plays an important role in the selection and design of molecular electrocatalysts for clean energy chemistry such as CO_2 reduction. Computational methods can aid catalyst design through predicting thermodynamic hydricities specifically through the use of Density Functional Theory (DFT). Although DFT is computationally efficient, the accuracy of DFT depends on the choice of various parameters including functional approximation, atomic basis set, and solvent model. In our study, we seek to benchmark and compare these parameters for their accuracy in predicting thermodynamic hydricities. We use ordinary least squares linear regression to map computed hydricity half-reaction free energies (ΔG_{HHR}) against experimentally determined hydricity values (ΔG_{H^-}) of various organic and organometallic hydride donors. Through the comparison of root-mean-squared errors, correlation coefficients, the slope, and intercept of the regression, we can judge the quality of a parameter set. Preliminary data shows that B3LYP performs better than BP86 and the larger TZVP-LTZ basis set performs better than 6-31G-LDZ. In addition, the data shows that the choice of functional is more important than the choice of basis set. Future work will include more molecules, functionals, basis sets, and solvent models to expand our benchmark.*

Introduction

The electrochemical reduction of CO_2 is an important direction of research to develop the renewable energy economy of the future. Generally speaking, CO_2 reduction involves the transfer of protons and electrons to the CO_2 molecule to produce reduced species such as formate anion, methanol, and methane. The reduction of CO_2 to formate in particular involves the transfer of a hydride (H^-) ion. The ability of these species to dissociate a hydride ion is defined as its thermodynamic hydricity. Hydricity plays an important role in catalytic design as the difference in the hydricity between the donor and acceptor, such as the catalyst and the formate ion, dictates the energy difference of that reaction being reduced dictates the energy barrier of that reaction and thus the ease the catalyst can reduce the target molecule. Many factors play in a molecule's hydricity including electronic, structural, and conformational; manipulating these factors can influence the hydricity. For example, Raebiger et al. demonstrated the ability to control the hydricity of palladium diphosphine complexes through the ligand bite angles¹.

The experimental measurement of thermodynamic hydricities is difficult and involves the use of multiple thermodynamic cycles, which involves taking sums and differences over the results of multiple experiments that form a thermodynamic pathway that connects the species of interest. To complement experiment, quantum chemical methods can also be used to predict hydricities. Ab initio or first-principles methods that treat the electrons in the system explicitly without empirical parameters such as coupled cluster singles and

double (CCSD) and 2nd order mller plesset perturbation theory MP2 have been used to study the thermodynamic hydricities of transition-metal hydrides in acetonitrile^{2,3}. More semi-empirical methods like density functional theory (DFT) have been employed in predicting the hydricity of an Ir based electrocatalyst⁴. Among the methods, DFT is popular in theoretical hydricity studies for its ability to achieve high accuracy without a high computational cost, however, the accuracy of a calculation depends on the choice of density functional approximations (here referred to as "functionals"), atomic basis sets, and solvent model for the system of interest. Developing functionals to achieve high accuracy for a specific system or classes of systems is a nontrivial task, so already established functionals that have been rigorously parameterized and tested are more commonly used. Examples of popular "all-purpose functionals" include B3LYP, PBE0, and M06 which all find use in theoretical studies of hydricity^{2,4-6}.

Although many functionals exist allowing flexibility in the accuracy and costs of performing hydricity calculations, the large "zoo" of functionals can overwhelm users. Because lack of a systematic way of improving density functionals unlike other quantum chemistry methods, many functionals have been developed to try to accurately simulate different systems of interest. Along with the choice of functional, users must also deal with the choice of atomic basis sets and solvent model. Generally, the larger the basis set, the more accurate the DFT calculation as more of the Hilbert space that describes the wavefunction is spanned. Additional factors also determine how well a basis set describes the electronic structure of a system such as including polarization functions to allow molecular orbitals to have more asymmetry or including diffuse functions to improve the description of atomic orbital at long distances from the atom. Another option to use in the choice of basis set are effective core potentials (ECPs) which replace the inner core electrons with an effective potential as they do not participate in chemical bonding as much as the valence electrons. An ECP can account for relativistic effects which are usually confined to the core electrons and serve to speed up calculations by reducing the number of electrons to calculate.

In addition to basis sets, the choice of solvent model is important to the accuracy of a calculation. The most accurate model would have solvent molecules explicitly present in the calculation, but this method is quite costly for quantum calculations and so implicit solvent models are more often used. Implicit solvent models generally represent the solvent as a continuous medium that has properties to replicate the interaction of the solvent(s) with the solute. A class of implicit model commonly used for hydricity calculations is the polarizable continuum model (PCM) where the medium is a polarizable medium⁷. C-PCM is a variation where the medium is a conductor like in the COSMO model⁸. Other examples of implicit solvent models include solvent model SMX⁹ and solvent model based on density SMD¹⁰.

For convenience, we will denote a combination of a functional, basis set, and solvent model as a parameter set. Because of the large number of combinations of these factors, benchmarks of functionals, atomic basis sets, and solvent models in predicting thermodynamic hydricity are necessary to determine the optimal parameter set. Benchmark studies are resource and time-consuming, but when conducted carefully, can be greatly helpful to other research groups interested in using density functional theory to study hydricity and problems such as CO₂ reduction. In our previous work on a four-centered iron electrocatalyst, we performed a small benchmark in the prediction of redox potentials with the 4 different functionals and 3 different atomic basis sets in acetonitrile¹¹.

In this study, we seek to establish a similar benchmark for predicting thermodynamic

hydricities with a larger range of functionals, atomic basis sets, and solvent models. Currently, we show that the hybrid B3LYP outperforms the GGA BP86 and that the larger TZVP-LTZ basis set outperforms 6-31G*-LDZ. In addition, we find that the choice of functional is more important than the choice of basis sets in terms of the impact on accuracy. We also show that optimizing the geometry of the benchmark molecules in the gas phase and running single point calculations in solvent does not predict hydricities significantly different from each other at the B3LYP/TZVP-LTZ level.

Methods

The hydricity of a hydride donating species, AH^- or BH , is defined as the standard free energy change of the following reactions.



In a solvent, we denote the hydricity with reaction 1a as:

$$\Delta G_{H^-}^*(AH^-) = G^*(A) + G^*(H^-) - \Delta G^*(AH^-) \quad (2)$$

where $\Delta G_{H^-}^*(AH^-)$ is the thermodynamic hydricity and the G^* values correspond to absolute free energies of the species indicated. The asterisk indicates a standard state of one mole per liter in solution to distinguish it from one atmosphere of pressure in the gas phase. More negative $\Delta G_{H^-}^*(AH^-)$ values imply a stronger hydride donating species.

Experimentally, the thermodynamic hydricity of a species is measured using thermodynamic cycles due to the difficulty in measuring the free energy value of solvated hydride ion, $G^*(H^-)$. Curtis and coworkers have measured the hydricities of transition metal complexes using a scheme based on equilibrium measurements for the heterolytic cleavage of hydrogen by transition metal complexes in the presence of bases for which the conjugate acid pKa values are known¹². Ilic and coworkers measured the hydricity of hydricity biomimetic organic hydride donors standard reduction potentials and pKa values to determine the results¹³.

Computationally, we can calculate each of the free energy terms in eq. 2 to derive the hydricity, but similarly to experiment, the difficulty of calculating the absolute free energy of solvated hydride ion precludes direct theoretical estimation as implicit solvent models fail to provide a good description of the solvent-hydride interaction. Previous ab initio approaches circumvented the calculation of this term through the use of an isodesmic scheme in which the experimentally derived hydricity value of a species is used as a reference². Another method uses a similar isodesmic scheme to calculate the relative hydricity values from a reference hydricity, $\Delta\Delta G_{H^-}^o$ to determine hydricity values¹⁴. Ilic et al. directly calculate the free energy of solvated hydride ion using calculated gas phase free energy and electron affinity values and experimental one-electron reduction potential of hydrogen¹³. A fourth method uses experimentally derived hydricity values and calculated values of $G^*(A)$ and $G^*(AH^-)$ to make $G^*(H^-)$ a fitting parameter. We follow this approach, described by Muckerman et al.¹⁵, by defining a "hydricity half reaction" (HHR) of the form:

$$\Delta G_{HHR}^* = G^*(A) - G^*(AH^-) \quad (3)$$

Substituting eq. 3 into the definition of hydricity in eq. 2 results in the following relation.

$$\Delta G_{H^-}^*(AH^-) = G_{HHR}^*(AH^-) + G^*(H^-) \quad (4)$$

We can use eq. 4 to plot calculated ΔG_{HHR} against experimentally derived G_{H^-} for each parameter set and use an ordinary least squares regression to fit G_{H^-} .

To ensure our benchmark covers a large range of hydride donating molecules and hydricities values, we use 30 organic and inorganic molecules with known experimental hydricity values in acetonitrile. 5 of these molecules come from Muckerman et al. paper in 2012¹⁵ so our benchmark can expand on their work. The measured hydricities span 25 years of literature from 1993 to 2018 and covers a variety of experimental techniques such as the potential-pKa method, the hydride transfer method, and H₂ heterolysis method described by Ilic and coworkers¹³. These methods generally employ measuring the free energy changes of various processes such as the dissociation of a proton and summing or subtracting the processes to calculate ΔG_{H^-} . These molecules are split between 15 organic and 15 inorganic hydride donors that cover a range of hydricities from 26 to 129.2 kcal/mol, although there is bias towards more experimentally available hydricity values for stronger hydride donors.

Table 1: Experimental hydricity values, ΔG_{H^-} for various organic and inorganic hydride donors in acetonitrile

Compound	Experimental ΔG_{H^-} (kcal/mol)	Compound	Experimental ΔG_{H^-} (kcal/mol)
BNAH	59 ^a	Cp*Re(NO)(CO)(CHO) ⁻	52.6 ^g
CN-BNAH	63 ^a	FeN(CO) ₁₂ H	49 ^h
Cp*Mo(PMe ₃)(CO) ₂ H	58 ^a	FeC(CO) ₁₂ H	44 ⁱ
CpMo(PMe ₃)(CO)2H	52.6 ^a	(Si(PiPr) ₃)Fe(H ₂)(H)	54.3 ^j
ArcH ₂	70 ^a	[HNi(dmpe) ₂] ⁺	48.9 ^k
Ph ₃ CH	99	[HPt(dmpp) ₂] ⁺	52.5 ^e
p-CN(Ph)CH ₃ CN	129.2 ^b	[HPd(depe) ₂] ⁺	43.2 ^l
HEH	61.5 ^c	HCo(dppe) ₂	49.1 ^e
2OH	60.3 ^c	HRh(depx) ₂	45 ^m
3NH	49.2 ^c	CpFe(CO) ₂ H	62 ⁿ
BIMH	50.1 ^c	Fluorene	109 ^o
BEt ₃ H ⁻	26 ^d	Toulene	118 ^o
[HNi(dedpe) ₂] ⁺	59.8 ^e	[HPd(PNP) ₂] ⁺	51.1 ^p
PhArcH	76.3 ^f	BMpyH	43 ^q
CpRe(NO)(CO)(CHO) ⁻	55 ^g	CHOO ⁻	44.2 ^r

a Ref. [16], b Ref. [17], c Ref. Ilic et al. [13], d Ref. [18], e Ref. [19], f Ref. [20], g Ref. [21], h Ref. [22], i Ref. [23], j Ref. [24], k Ref. [25], l Ref. [1], m Ref. [26], n Ref. [27], o Ref. [28], p Ref. [29], q Ref. [30], r Ref. [31]

Computational Methods

All calculations were carried out using TeraChem³² which uses graphics processing units to accelerate the computation of the coulomb and exchange matrices, ECPs, and solvent response that appear in the SCF calculation.

$$G = G_{solv} + E_{SCF} + ZPE + H_{tr,vib,rot} - TS_{tr,rot,vib} \quad (5)$$

In TeraChem, the Gibbs free energy for a solvated species is defined in eq. 5. To calculate the values in eq. 5 we employ two optimization schemes. In the first scheme, we use geometry optimization methods using translation-rotation internal coordinates to accelerate the energy minimization calculations³³. Geometry optimization was used to derive the self-consistent field (SCF) electronic energy together with the solvation free energy. Vibrational frequency calculations were used to derive the zero point energy and Gibbs free energy contributions within the harmonic approximation which assumes that the vibrational enthalpy and entropy of a molecule is well-described using a set of harmonic oscillators obtained from the normal modes.

For the parameter sets examined, eight combinations of functionals (B3LYP and BP86), basis sets (6-31G*-LDZ and TZVP-LDZ), and solvent model (C-PCM and Gas Phase) were examined for this paper. The solvent was chosen to replicate acetonitrile by giving the medium a dielectric constant, ϵ , of 37.5. The basis sets have the addition of -LDZ/-LTZ to designate that the LANL2DZ/LANL2TZ basis set and associated ECP was used for elements from Sc and heavier.

For the calculations, geometry optimization at the eight levels of theory discussed was ran for all thirty molecules in table 1 for their hydride donor and hydride conjugate acceptor, however, some calculations for either the donor or acceptor were not complete or failed leading to some incomplete data. For statistical analysis, ordinary linear regression was performed and summarized in table 2. The most likely spin state of the donor and acceptor was determined through running calculations on each molecule at different spin states and selecting the calculations that gave the lowest free energy values.

In addition to the first scheme where all values in eq.3 were calculated using geometry optimization for all 8 parameter sets, the second scheme we employ involves performing single point calculations with C-PCM with the structures that were optimized in the gas phase from the first scheme. We employ these two optimization schemes to evaluate whether the calculated G_{solv} and H_{SCF} differ significantly. For the comparison, we assume that the frequency corrections in eq. 5 are small therefore we use the same frequency corrections of the structure that was geometry optimized in solvent phase and compare ΔG_{HHR} values.

Results and Discussion

Comparison between optimization schemes

We start our discussion of the calculations with the comparison of the ΔG_{HHR} values using the geometry optimization schemes in the gas phase and solvent phase. Because the calculation for either the hydride donor or acceptor failed for $\text{HCo}(\text{dppe})_2$, $\text{CpRe}(\text{NO})(\text{CO})(\text{CHO})^-$, and $\text{Cp}^*\text{Re}(\text{NO})(\text{CO})(\text{CHO})^-$, they were not able to be included in the comparison. We plot the calculated ΔG_{HHR} from both optimization schemes against each other and evaluate how close to unity the slope and r^2 of a linear regression of the plot are for comparison. The frequency contributions are small so we use the frequency calculations from solvent phase geometry optimization to calculate ΔG_{HHR} for a single point calculation.

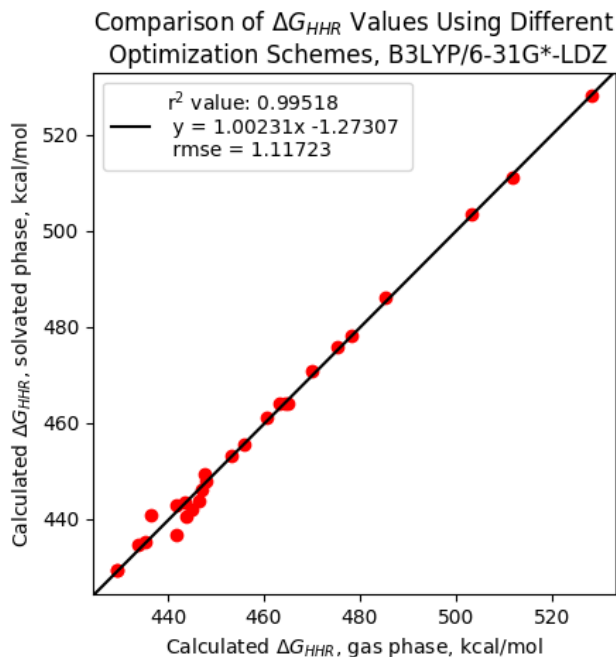


Figure 1: Comparison of calculated ΔG_{HHR} values of 27 organic and inorganic hydride donating molecules from both optimization schemes. Data points for $\text{HCo}(\text{dppe})_2$, $\text{CpRe}(\text{NO})(\text{CO})(\text{CHO})^-$, and $\text{Cp}^*\text{Re}(\text{NO})(\text{CO})(\text{CHO})^-$ were not included as calculations for these molecules were incomplete. The r^2 and slope are both close to 1 indicating that performing single point calculations for G_{solv} and E_{SCF} in solvent phase using gas phase geometry optimized structures does not produce significant differences from geometry optimization calculations for G_{solv} and E_{SCF} in solvent phase.

The calculated ΔG_{HHR} values from both optimization schemes in fig. 1 show close agreement as the linear regression has a r^2 and a slope very close to unity. Fig. 1 indicates that running a single point calculation in the solvated phase using structures that were geometry optimized in gas phase does not differ significantly. The lack of a significant difference can be used as partial justification to run other levels of theory using the geometry optimized structures from the least expensive B3LYP/6-31G*-LDZ/Gas level of theory. Further calculations to generate figures such as fig. 1 with different parameter sets need to be made before full justification. If no significant difference is found between the schemes in calculating ΔG_{HHR} , using single point method with geometries optimized at lower levels of theory can be partially justified thereby expediting calculations as geometry optimizations are much more costly.

Some features to note in fig. 1 include that points with lower calculated ΔG_{HHR} values show more deviation from the trend. We hypothesize that these deviations result from statistical variation being more prevalent near those regions as there are more molecules in the lower ΔG_{HHR} ranges. If there were more molecules that are weaker hydride donors (higher ΔG_{HHR}) included in our study there would also be more data points that vary from the linear regression. A larger number of stronger hydride donors than weaker hydride donors were included in this study as there are more of stronger hydride donors with experimentally determined ΔG_{H^-} values in the literature.

Future plans will run more calculations as described, but this preliminary result indicates that those calculations will generate similar results as the difference in G_{solv} and H_{SCF} is not that large across different levels of theory. In addition, the 3 molecules whose

ΔG_{HHR} values that did not finish will be also calculated.

Comparison of Linear Regressions For Eight Parameter Sets

Because the comparison between the optimization schemes is not complete, we will compare the different linear regressions according to eq. 4 for the B3LYP/BP86, 6-31G*-LDZ/TZVP-LTZ, and C-PCM/Gas functionals, basis sets, and solvent models. Due to 5 molecules across each of the eight calculations having incomplete calculations, only 25 molecules will be included in the analysis. The molecules not included are $\text{FeN}(\text{CO})_2$, $\text{HCo}(\text{dppe})_2$, $\text{Si}(\text{PiPr})_3\text{Fe}(\text{H}_2)(\text{H})$, $\text{CpFe}(\text{CO})_2\text{H}$, and $\text{HRh}(\text{depx})_2$.

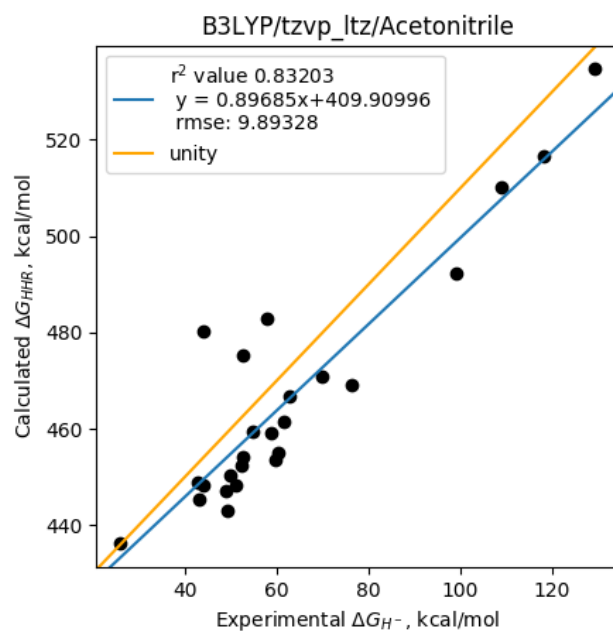


Figure 2: Correlation between calculated $\Delta G_{HHR}(H^-)$ and experimental ΔG_{H^-} at the B3LYP/TZVP-LTZ level with C-PCM model for acetonitrile

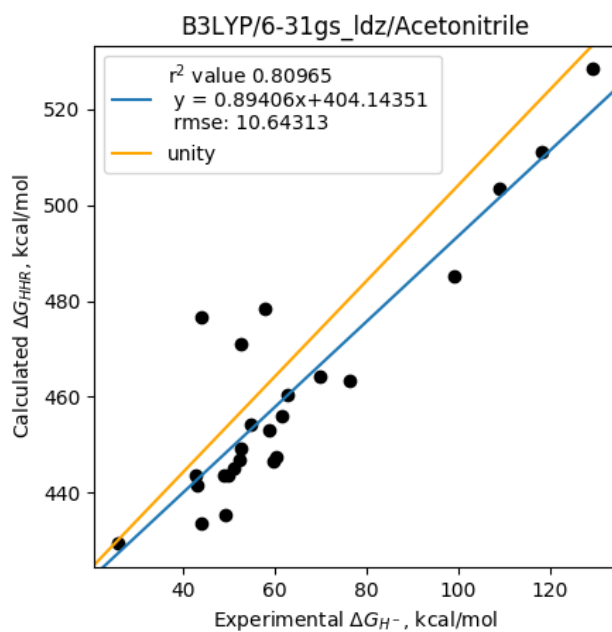


Figure 3: Correlation between calculated $\Delta G_{HHR}(H^-)$ and experimental ΔG_{H-} at the B3LYP/6-31G*_ldz level with C-PCM model for acetonitrile

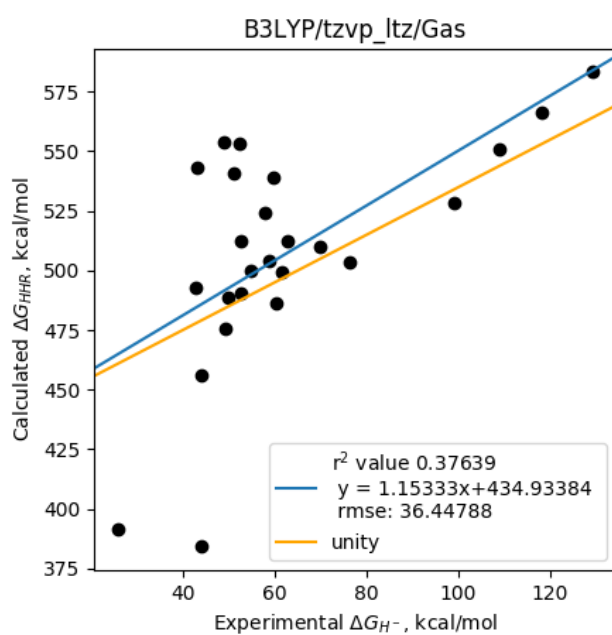


Figure 4: Correlation between calculated $\Delta G_{HHR}(H^-)$ and experimental ΔG_{H-} at the B3LYP/TZVP-LTZ level at gas phase.

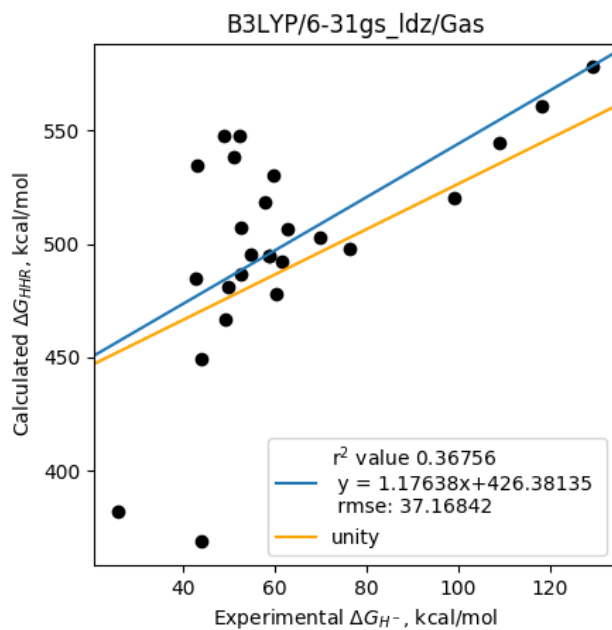


Figure 5: Correlation between calculated $\Delta G_{HHR}(H^-)$ and experimental ΔG_{H^-} at the B3LYP/6-31G*_ldz level at gas phase.

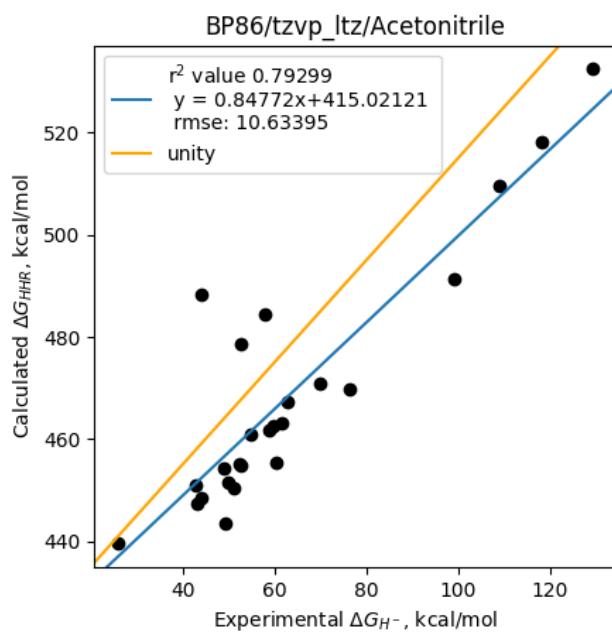


Figure 6: Correlation between calculated $\Delta G_{HHR}(H^-)$ and experimental ΔG_{H^-} at the BP86/TZVP-LTZ level with C-PCM model for acetonitrile

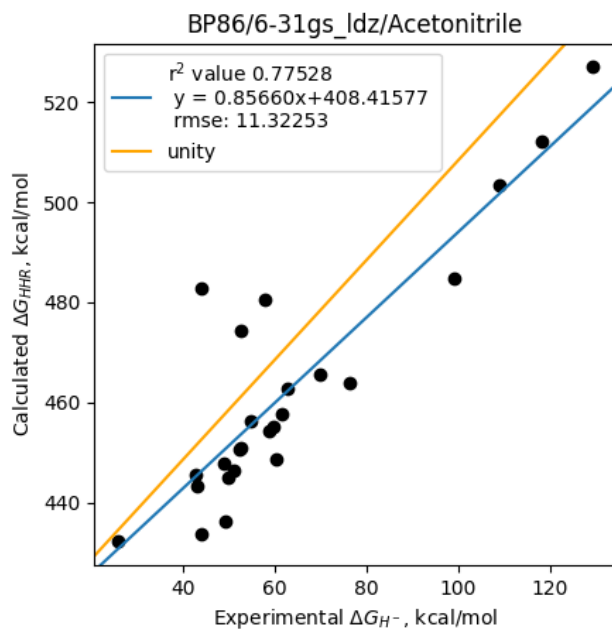


Figure 7: Correlation between calculated $\Delta G_{HHR}(H^-)$ and experimental ΔG_{H-} at the BP86/6-31G*_ldz level with C-PCM model for acetonitrile

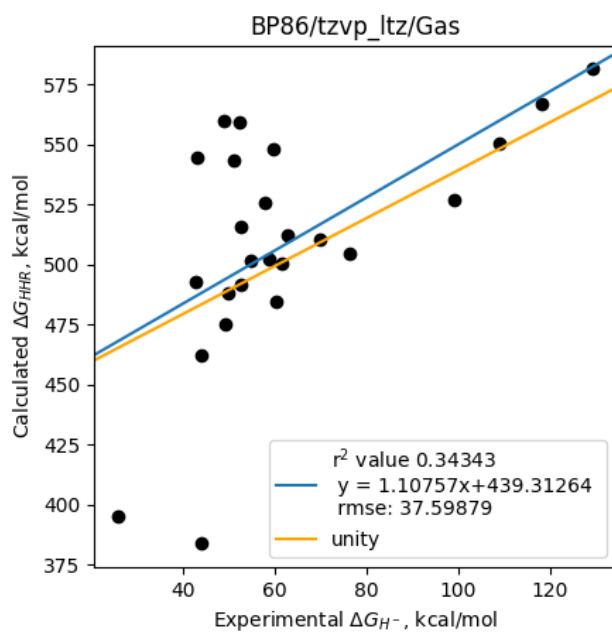


Figure 8: Correlation between calculated $\Delta G_{HHR}(H^-)$ and experimental ΔG_{H-} at the BP86/TZVP-LTZ level at gas phase.

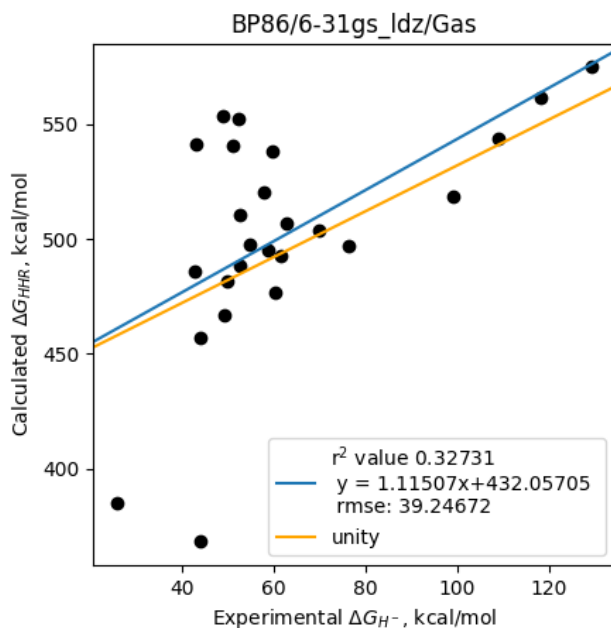


Figure 9: Correlation between calculated $\Delta G_{HHR}(H^-)$ and experimental ΔG_{H-} at the BP86/6-31G*_ldz level at gas phase.

Table 2: Summary of linear regression analysis of calculated ΔG_{HHR} against ΔG_{H-} ordered by lowest to higher RMSE values.

Functional	Basis	Solvent	RMSE	r ² value	Slope	Intercept
B3LYP	TZVP-LTZ	Acetonitrile	9.893	0.832	0.8968	409.9
BP86	TZVP-LTZ	Acetonitrile	10.634	0.793	0.8477	415.0a
B3LYP	6-31G*-LDZ	Acetonitrile	10.643	0.8097	0.8941	404.1
BP86	6-31G*-LDZ	Acetonitrile	11.323	0.7753	0.8566	408.4
B3LYP	TZVP-LTZ	Gas	36.448	0.3764	1.1533	434.9
B3LYP	6-31G*-LDZ	Gas	37.168	0.3676	1.1764	426.4
BP86	TZVP-LTZ	Gas	37.599	0.3434	1.1076	439.3
BP86	6-31G*-LDZ	Gas	39.247	0.3273	1.1151	432.1

Starting by evaluating the performance of the different solvent models in figs. 2 to 9, the gas phase calculations perform worse than the calculations that used the C-PCM model. This result is not surprising as one would expect not including the solvent in the calculations would reproduce inaccurate ΔG_{HHR} values as the solvent-solute interactions are missing. The poor performance of the gas phase calculations can be seen in table 2.

Within the acetonitrile linear regressions, it can be visually noted that three data points in figs. 6, 7, 2, and 7, consistently deviate from the linear regression. A reason why these points deviate is that some of the calculations are in a transition state and the geometry optimization algorithm used is unable to climb out of the saddle point. These saddles points are most likely near the global minimum as the geometries of the molecules used here were obtained from literature and x-ray crystallography data. An improvement that

could be made to improve the linear regression would be to perturb the geometries around the saddle point and run geometry optimizations until the molecule moves to a minimum on the potential energy surface. This process has been attempted for molecules on the saddle point, but no success in reaching minima has been made up until this point. More efforts and techniques in this issue will be made and explored. Another potential reason for the deviation is that the literature values may contain errors in the experimental measurement.

Moving to compare functionals and basis sets, B3LYP consistently outperforms BP86 as shown in table 2. This result hints that hybrid functionals like B3LYP outperform generalized gradient approximation (GGA) functionals like BP86 for predicting hydricities, but full confidence in this claim cannot be recommended without testing more functionals. In comparing the basis sets the larger TZVP-LTZ basis set performs better than the smaller 6-31G*-LDZ basis set although the magnitude of the improvement in the accuracy is not as large as changing the functionals.

Overall, the best theory to run hydricity calculations amongst the eight sets is B3LYP/TZVP-LTZ with C-PCM with $\epsilon = 37.5$ as this level of theory and solvent model has the lowest RMSE and r^2 and slope values closest to unity. The extrapolated intercept value, $G^*(H^-)$, is relatively close to the literature which have theoretical predicted the value of $G^*(H^-)$ in acetonitrile at -400.7 and -404.7 kcal/mol^{14,34}. In the evaluation of the hierarchy of importance of the functional, basis set, and solvent model, only comparisons between two functionals and two basis sets can be made as only one solvent model was examined. Future plans will examine more solvent models such as D-PCM, SMD, and SM12 so that a conclusion on the relative importance of the solvent model to the other two factors can be made. Comparing functionals to basis sets show that the choice of functional is more important than the choice of basis set as B3LYP/TZVP-LTZ and B3LYP/6-31G*-LDZ outperform BP86/TZVP-LTZ and BP86/6-31G*-LDZ. We make this claim as even though BP86/TZVP-LTZ has a lower RMSE value than B3LYP/6-31G*-LDZ, the r^2 , slope, and intercept values are better for B3LYP/6-31G*-LDZ. Slope values should ideally be 1.0 since ΔG_{HHR} is related to ΔG_{H-} by a constant. That the slopes deviate from 1.0 indicates some systematic error in our assumptions and calculations.

Future work will include evaluating a larger set of functionals from different classes according to the hierarchy following Jacob’s ladder described by Rappaport et al. in which they rank functional classes by GGA>meta-GGA>hybrid>fully nonlocal functionals³⁵. We will examine more GGA, meta-GGA, hybrid, and fully nonlocal functionals in the future. We predict that the accuracy of the hydricity calculations will follow the hierarchy discussed, but hope to see surprising results. More basis sets will also be examined such as larger Pople³⁶, Dunning³⁷, and Karlsruhe³⁸ basis sets. We expect that larger basis sets will lead to more accurate hydricity predictions. In addition, we seek to further compare the effects of using an ECP vs not using an ECP as well as comparing different ECPs. The effects of using the ECP will only be relevant for compounds that contain heavier elements. Since the ECP only replace core electrons which that do not interact with the solvent as much as the valence electrons we expect that an all-electron calculation will not significantly improve the calculated hydricity values and will make calculations more expensive. To further improve the extent of our benchmark, we plan to include more hydride donors. Along with the parameters, we also will look into calculating hydricity values in other solvents such as water and DMSO although experimentally determined hydricity values in those solvents are harder to find in literature.

Conclusion

In this study, we compare how well DFT calculations with different sets of functionals, atomic basis sets, and solvent models predict hydricity values using 30 molecules with experimentally measured hydricities taken from the literature. Preliminary results suggest that using gas phase geometry optimized structures for each molecule can be used in place of geometry optimizing the molecule in solvent, but more data is needed to confirm this claim. We compared eight sets consisting of a combination of two functionals, two basis sets, and two solvent models. We conclude that using the B3LYP functional performs better than BP86 and that using the larger TZVP-LTZ basis set does better than 6-31G*-LDZ. We determined of all the parameters examined, the linear regression for B3LYP/TZVP-LTZ with the C-PCM solvent model yielded a RMSE of 9.893 kcal/mol, r^2 of 0.832, slope of 0.8968, and intercept of 409.9 kcal/mol. In addition, preliminary data shows that it is important to use a solvent model to correctly predict hydricity values and that the choice of functional precedes choice of basis set. For future plans, we seek to expand our study to include more molecules, functionals, basis set, solvent models, solvents, and ECPs toward the goal of contributing a widely useful benchmark study to the literature.

References

- (1) Raebiger, J. W.; Miedaner, A.; Curtis, C. J.; Miller, S. M.; Anderson, O. P.; DuBois, D. L. *Journal of the American Chemical Society* **2004**, *126*, 5502–5514.
- (2) Qi, X.-J.; Fu, Y.; Liu, L.; Guo, Q.-X. *Organometallics* **2007**, *26*, 4197–4203.
- (3) YU, A.; WANG, H.-K.; XUE, X.-S.; CAI, Y.; WANG, Y.-J.; HE, J.-Q. *Chemical Journal of Chinese Universities* **2012**, *10*.
- (4) Garg, K.; Matsubara, Y.; Ertem, M. Z.; Lewandowska-Andralojc, A.; Sato, S.; Szalda, D. J.; Muckerman, J. T.; Fujita, E. *Angewandte Chemie International Edition* **2015**, *54*, 14128–14132.
- (5) Wu, P.; Du, P.; Zhang, H.; Cai, C. *The Journal of Physical Chemistry C* **2012**, *116*, 20472–20479.
- (6) Vasic, D. D.; Pasti, I. A.; Mentus, S. V. *International Journal of Hydrogen Energy* **2013**, *38*, 5009–5018.
- (7) Cossi, M.; Barone, V.; Cammi, R.; Tomasi, J. *Chemical Physics Letters* **1996**, *255*, 327–335.
- (8) Amovilli, C.; Barone, V.; Cammi, R.; Cancès, E.; Cossi, M.; Mennucci, B.; Pomelli, C. S.; Tomasi, J. In *Advances in Quantum Chemistry*; Elsevier: 1998; Vol. 32, pp 227–261.
- (9) Liu, J.; Kelly, C. P.; Goren, A. C.; Marenich, A. V.; Cramer, C. J.; Truhlar, D. G.; Zhan, C.-G. *Journal of chemical theory and computation* **2010**, *6*, 1109–1117.
- (10) Marenich, A. V.; Cramer, C. J.; Truhlar, D. G. *The Journal of Physical Chemistry B* **2009**, *113*, 6378–6396.
- (11) Jang, H.; Qiu, Y.; Hutchings, M. E.; Nguyen, M.; Berben, L. A.; Wang, L.-P. *Chemical science* **2018**, *9*, 2645–2654.
- (12) Curtis, C. J.; Miedaner, A.; Ellis, W. W.; DuBois, D. L. *Journal of the American Chemical Society* **2002**, *124*, 1918–1925.

- (13) Ilic, S.; Pandey Kadel, U.; Basdogan, Y.; Keith, J. A.; Glusac, K. D. *Journal of the American Chemical Society* **2018**, *140*, 4569–4579.
- (14) Nimlos, M. R.; Chang, C. H.; Curtis, C. J.; Miedaner, A.; Pilath, H. M.; DuBois, D. L. *Organometallics* **2008**, *27*, 2715–2722.
- (15) Muckerman, J. T.; Achord, P.; Creutz, C.; Polyansky, D. E.; Fujita, E. *Proceedings of the National Academy of Sciences* **2012**, *109*, 15657–15662.
- (16) Ellis, W. W.; Raebiger, J. W.; Curtis, C. J.; Bruno, J. W.; DuBois, D. L. *Journal of the American Chemical Society* **2004**, *126*, 2738–2743.
- (17) Zhang, X.-M.; Bruno, J. W.; Enyinnaya, E. *The Journal of Organic Chemistry* **1998**, *63*, 4671–4678.
- (18) DuBois, D. L.; Blake, D. M.; Miedaner, A.; Curtis, C. J.; DuBois, M. R.; Franz, J. A.; Linehan, J. C. *Organometallics* **2006**, *25*, 4414–4419.
- (19) Berning, D. E.; Noll, B. C.; DuBois, D. L. *Journal of the American Chemical Society* **1999**, *121*, 11432–11447.
- (20) Yang, X.; Walpita, J.; Zhou, D.; Luk, H. L.; Vyas, S.; Khnayzer, R. S.; Tiwari, S. C.; Diri, K.; Hadad, C. M.; Castellano, F. N., et al. *The Journal of Physical Chemistry B* **2013**, *117*, 15290–15296.
- (21) Ellis, W. W.; Miedaner, A.; Curtis, C. J.; Gibson, D. H.; DuBois, D. L. *Journal of the American Chemical Society* **2002**, *124*, 1926–1932.
- (22) Taheri, A.; Thompson, E. J.; Fettingner, J. C.; Berben, L. A. *ACS Catalysis* **2015**, *5*, 7140–7151.
- (23) Taheri, A.; Berben, L. A. *Inorganic chemistry* **2015**, *55*, 378–385.
- (24) Fong, H.; Peters, J. C. *Inorganic chemistry* **2014**, *54*, 5124–5135.
- (25) Berning, D. E.; Miedaner, A.; Curtis, C. J.; Noll, B. C.; Rakowski DuBois, M. C.; DuBois, D. L. *Organometallics* **2001**, *20*, 1832–1839.
- (26) Raebiger, J. W.; DuBois, D. L. *Organometallics* **2005**, *24*, 110–118.
- (27) Estes, D. P.; Vannucci, A. K.; Hall, A. R.; Lichtenberger, D. L.; Norton, J. R. *Organometallics* **2011**, *30*, 3444–3447.
- (28) Cheng, J.; Handoo, K. L.; Parker, V. D. *Journal of the American Chemical Society* **1993**, *115*, 2655–2660.
- (29) Curtis, C. J.; Miedaner, A.; Raebiger, J. W.; DuBois, D. L. *Organometallics* **2004**, *23*, 511–516.
- (30) Matsubara, Y.; Fujita, E.; Doherty, M. D.; Muckerman, J. T.; Creutz, C. *Journal of the American Chemical Society* **2012**, *134*, 15743–15757.
- (31) Miller, A. J.; Labinger, J. A.; Bercaw, J. E. *Organometallics* **2011**, *30*, 4308–4314.
- (32) Ufimtsev, I. S.; Martinez, T. J. *Journal of Chemical Theory and Computation* **2009**, *5*, 2619–2628.
- (33) Wang, L.-P.; Song, C. *The Journal of chemical physics* **2016**, *144*, 214108.
- (34) Kovacs, G.; Papai, I. *Organometallics* **2006**, *25*, 820–825.
- (35) Rappoport, D.; Crawford, N. R.; Furche, F.; Burke, K.; Wiley, C. *Computational Inorganic and Bioinorganic Chemistry* **2008**, 594.

- (36) Ditchfield, R.; Hehre, W. J.; Pople, J. A. *The Journal of Chemical Physics* **1971**, *54*, 724–728.
- (37) Dunning Jr, T. H. *The Journal of chemical physics* **1989**, *90*, 1007–1023.
- (38) Schafer, A.; Horn, H.; Ahlrichs, R. *The Journal of Chemical Physics* **1992**, *97*, 2571–2577.